Top Catal (2016) 59:516–525
DOI 10.1007/s11244-015-0520-8

ORIGINAL PAPER

The Partial Oxidation of Methane Over Pd/Al_2O_3 Catalyst Nanoparticles Studied In-Situ by Near Ambient-Pressure X-ray Photoelectron Spectroscopy

Rachel Price[1] · Tuğçe Eralp-Erden[2] · Ethan Crumlin[3] · Sana Rani[3] · Sonia Garcia[2] · Richard Smith[2] · Liam Deacon[4] · Chanan Euaruksakul[1,4] · Georg Held[1,4]

Published online: 19 January 2016

Abstract Near ambient-pressure X-ray photoelectron spectroscopy (NAP-XPS) is used to study the chemical state of methane oxidation catalysts in-situ. Al_2O_3–supported Pd catalysts are prepared with different particle sizes ranging from 4 to 10 nm. These catalysts were exposed to conditions similar to those used in the partial oxidation of methane (POM) to syn-gas and simultaneously monitored by NAP-XPS and mass spectrometry. NAP-XPS data show changes in the oxidation state of the palladium as the temperature increases, from metallic Pd^0 to PdO, and back to Pd^0. Mass spectrometry shows an increase in CO production whilst the Pd is in the oxide phase, and the metal is reduced back under presence of newly formed H_2. A particle size effect is observed, such that CH_4 conversion starts at lower temperatures with larger sized particles from 6 to 10 nm. We find that all nanoparticles begin CH_4 conversion at lower temperatures than polycrystalline Pd foil.

Keywords Pd catalyst · Methane oxidation · Alumina support · X-ray photoelectron spectroscopy

1 Introduction

Instead of flaring off large quantities of unused natural gas around the world, it could be used in a more environmentally friendly way as fuel for automotive engines. Natural gas vehicles (NGVs) operate under lean conditions with low methane concentrations (500–1000 ppm) and working temperatures typically under 823 K (550 °C). The beneficial outcome of these working conditions is that relatively "clean" products are produced (CO_2, H_2, H_2O) in comparison to other fossil fuels producing harmful nitrogen and sulphur containing compounds. In NGVs, NO_x and SO_x exhaust emissions are greatly reduced [1–3]. The challenge lies with the storage and transport of gases, and the conversion into a more useful, transportable product. The C–H bonds in aliphatic hydrocarbons have high dissociation energies (439.3 kJ mol^{-1} in CH_4) and the absence of functional groups leaves the molecule with zero polarity and no sites for either nucleophilic or electrophilic attack. This makes small hydrocarbons, such as methane, very difficult to oxidise without a catalyst at low temperatures [4].

The partial oxidation of methane (POM) uses an oxygen-deficient mixture to produce carbon monoxide and hydrogen:

$$CH_4 + \frac{1}{2}O_2 \rightarrow CO + 2H_2$$

This CO/H_2 mixture (commonly known as "syn-gas") is a useful precursor for methanol synthesis. Methanol is a versatile, clean-burning liquid that is used in many

Electronic supplementary material The online version of this article (doi:10.1007/s11244-015-0520-8) contains supplementary material, which is available to authorized users.

✉ Georg Held
g.held@reading.ac.uk

[1] Department of Chemistry, University of Reading, Reading RG6 6AD, UK

[2] Johnson Matthey Technology Centre, Blounts Court Road Sonning Common, Reading RG4 9NH, UK

[3] Advanced Light Source Lawrence Berkeley National Laboratory, Berkeley, CA 94720, USA

[4] Diamond Light Source Harwell Science and Innovation Campus, Didcot OX11 0QX, UK

applications, including in the production of animal feed, hydrogen storage and as a precursor for the octane-enhancing additive methyl–tertiary–butyl ether (MTBA) [5]. Moreover, methanol in itself has the potential to become a large-scale renewable alternative to fossil fuels [6]. It is produced by the hydrogenation of CO at 773–923 K commercially using a $Cu/ZnO/Al_2O_3$ catalyst [7]:

$$CO + 2H_2 \rightarrow CH_3OH$$

Syn-gas is not currently produced on a large scale by partial methane oxidation, but instead by steam-reforming, where methane reacts with water, over a nickel-based catalyst, at high temperatures (>1000 K) and pressures [8]:

$$CH_4 + H_2O \rightarrow CO + 3H_2$$

Although this is a high-yielding reaction, the conditions at which it operates are expensive and unsustainable in the long term. Therefore it is of great importance to find a viable catalyst to enable large-scale POM for syn-gas production at lower temperatures and atmospheric pressures. POM reaction conditions are generally leaner and more cost effective than those of steam reforming. It has previously been reported that the syn-gas yield and selectivity is optimised with temperatures above 650 K [9, 10] (a 90 % yield is observed at 1050 K with a variety of transition metal-based catalysts [11]). For both methane oxidation and steam-reforming, a catalyst is yet to be developed that can activate this reaction at sustainable and more cost effective, lower temperatures and pressures.

Platinum group metals are widely used as the basis for catalysts for a number of different applications [12]. In particular, Pd and Pt are used for methane activation reactions, in the form of supported nanoparticles. The mechanism by which they operate is still relatively unknown. It has been established that a change in oxidation state of the metal occurs, but in the case of palladium-based catalysts, it is unclear as to which state is the active species. Burch et al. [13] reported that for a Pd catalyst the fully oxidized surface is the optimum state, but more recently Yang et al discovered that a mixed phase of PdO and PdO_x (where $0 < x \leq 1$) is the most active state for methane combustion [14]. For the Pd(111) surface, it has been reported that a 2D surface oxide, Pd_5O_4, forms after exposure to oxygen at high temperatures [15].

X-ray photoelectron spectroscopy (XPS) is a useful, surface sensitive technique for identifying the surface chemical state and composition of solids. In order to avoid unintentionally measuring contaminants rather than the species of interest, these experiments are generally performed in an ultra-high vacuum (UHV). However, in catalysis, UHV is not a representative condition and a catalyst under UHV conditions may behave differently compared to reaction conditions. Near ambient-pressure (NAP-) XPS helps to bridge this gap, with pressures up to 100 Torr (130 mbar) now possible [16]. The differential pumping of NAP-XPS systems gradually reduces the pressure in the analysis chamber down to UHV at the analyser [17], and so it is possible to collect information about the chemical state of the surface of the catalyst in-situ, under specific close-to-real-world reaction conditions.

2 Experimental

2.1 Sample Preparation

Several samples of 5 wt% γ-Al_2O_3 supported Pd nanoparticles were prepared by the co-precipitation method [18], using a $Pd(NO_3)_2$ precursor (8.34 % assay, Alfa-Aesar). A solution of dodecenyl succinic anhydride (DSA) in THF was added to a base solution of aqueous Na_2CO_3. Aqueous palladium nitrate was added to the flask dropwise in molar excess and γ-Al_2O_3 was added as the support material. The resulting slurry was filtered under suction, prior to drying in the oven for 2 hours at 380 K and calcination treatment. The nanoparticles were crushed and calcined for 2 h in air at a range of temperatures between 300 and 700 °C (573–973 K) in order to achieve a range of particle sizes (see Table 1).

Catalysts A (4 nm), B (5 nm), C (6 nm), D (7 nm) and E (10 nm) were chosen as the samples used for these experiments, to give a representative size range. 1 g of Pd/Al_2O_3 nanoparticles and 0.1 g of P3 (to improve adhesion) was added to 3 g H_2O. A P-doped silicon wafer (1 cm^2) was fixed to a hot plate and the nanoparticles were deposited onto the wafer using a spray gun. Each spray lasted for five seconds and the silicon wafers were weighed before and after. The water evaporated off to leave a dry, homogeneous layer of Pd/Al_2O_3 nanoparticles.

2.2 Sample Characterisation

Laboratory-based XPS was used to determine the elemental composition of the catalysts. The Pd/Al_2O_3 nanoparticles were mounted onto adhesive carbon tape and inserted into a Thermo Escalab 250 photoelectron spectrometer, which is equipped with a monochromatised Al K-α source ($h\nu$ = 1486.6 eV) with a large spot to maximise count rate, a flood gun, and an electromagnetic lens. The nanoparticles were probed to identify surface elemental composition at room temperature and ultra-high vacuum (base pressure 10^{-8} mbar). Overview spectra determined the levels of contamination and high-resolution spectra

Table 1 List of samples prepared

Catalyst	Calcination (K)	Mean d_{TEM} (nm)	σ (nm)	MSA (m^2/g)	MD (%)
A (4 nm)	573 (300 °C)	4.06	1.23	0.29	1.30
B (5 nm)	773 (500 °C)	4.91	1.54	0.15	0.69
C (6 nm)	873 (600 °C)	6.16	1.56	0.13	0.57
D (7 nm)	973 (700 °C)	7.12	1.86	0.18	0.80
E (10 nm)	873 (600 °C)[a]	9.63	1.98	–	–

The mean diameter of Pd/Al_2O_3 nanoparticles calcined to different temperatures as determined by TEM, metal surface area (MSA) and % metal dispersion (MD) as determined from CO chemisorption

[a] Batch prepared in a previous study; used here to complete the particle size range

obtained in the Pd 3d, O 1s, and Al 2p regions confirmed the relative presence and oxidation state of each element. Spectra taken in the Pd 3d region suggest the nanoparticles are in their oxidised state, with Pd $3d_{5/2}$ peaks at 336 eV representative of a PdO species. This is to be expected as alumina has Lewis acid sites on the surface, rendering the metal electron-deficient and increasing the oxidation state [19]. The electron-deficient Pd^{2+} species is then free to bond with oxygen atoms from the air, resulting in PdO.

Transmission electron microscopy (TEM) was used to determine the mean particle size of each synthesised sample (Fig. 1 of Supporting Information). The samples were each ground between two glass slides and dusted onto a holey carbon coated copper grid prior to examination in a Tecnai F20 transmission electron microscope. The samples were analysed using 200 kV and 30 μm C2 aperture at a variety of magnifications ranging from 5 to 100 nm. Approximately 100 nanoparticles in each sample were measured at different magnifications and in different areas to gain a representative mean particle size.

The metal surface area and % metal dispersion were measured using a Micromeritics AutoChem II 2920 analyser. Pulses of CO were passed through 0.1 g of catalyst sample at 308 K and the adsorbed CO was determined by a thermal conductivity detector. A reduction step prior to the CO pulses ensured that all the palladium had been reduced to a metallic state. The surface area of palladium in each catalyst is given by:

$$\text{Area of Pd} = \frac{\text{molecules of CO adsorbed}}{\text{molecules per m}^2}$$

The percentage metal dispersion is calculated using:

$$\text{MD}(\%) = \frac{N_S}{N_T} \times 100$$

where N_S is the number of atoms on the surface and N_T is the total number of atoms in the sample. The results are shown in Table 1.

The reactivity of Pd/Al_2O_3 catalysts A (4 nm), B (5 nm), D (7 nm) and E (10 nm) was tested using a batch flow reactor (Johnson Matthey, Fig. 2 of Supporting Information). Each catalyst was pressed into a pellet, crushed and sieved at 250–355 μm. Under a constant flow of air, 0.4 g of each catalyst was exposed to 1000 ppm of methane and various concentrations of pure O_2 (1, 5, 12 %) as the temperature was ramped from 400 to 800 K (ramp rate 10 K/min). The y-axis (% CH_4 conversion) is calculated based on the amount of CO and CO_2 observed as a function of temperature. The data show that there is very little difference between the light-off temperatures when different sized nanoparticles and $[CH_4] : [O_2]$ ratios are used in these concentrations, with the exception of 10 nm nanoparticles which begin methane conversion at almost 100 K lower. Catalyst E is the only catalyst to reach 100 % conversion before 800 K, suggesting they are the most active nanoparticles.

2.3 Synchrotron Experiments

Near ambient-pressure XPS studies were carried out at beam line 9.3.2 of the Advanced Light Source (ALS), National Lawrence Berkeley Laboratory, USA [20]. The endstation is equipped with a Scienta 4000 HiPP analyser with a custom designed differential pumping system that allows pressures of up to 1 Torr in the analysis chamber, enabling in-situ data collection. A mass spectrometer is placed in the first differential pumping stage, which was used to quantify the gas composition during the reaction. The samples were individually mounted onto a UHV compatible sample holder connected to thermocouple wires for controlled heating.

Each sample was fully characterised by XPS in UHV at 450 K, a temperature at which the sample is much less affected by charging than at room temperature (Figure 3 of Supporting Information), before being exposed to a 240 mTorr gaseous mixture of oxygen and methane ($[CH_4] : [O_2] = 2$). The temperature of the sample was increased in steps of 50 or 100 K between 400 and 700 K. In-situ high-resolution XPS measurements were taken at constant temperature during this temperature ramp. Pd 3d, Al 2p and C 1s spectra were obtained using the same incident photon energy of $h\nu = 450$ eV, with the binding

energies being calibrated to the literature value for Al 2p (74.5 eV). QMS data were collected throughout the XPS measurements.

The NAP-XP spectra obtained were normalised and a Shirley background [21] was subtracted. The difference in binding energy between the literature value of the Al 2p peak (74.5 eV [22]) and the experimental value was determined and applied to correct the binding energy scale of the corresponding Pd 3d and C 1s spectra. This is based on the assumption that, both Pd and C, sitting on the Al_2O_3 support are affected by the same charging shifts. Although not proving to be a problem for data collection, the lack of sample conductivity occasionally broadens the Al 2p peak. The extent to which these peaks broaden is taken into account when fitting the corresponding Pd 3d peaks. In some cases, where sample charging was inhomogeneous, the Al 2p peak is split into two. Each Pd 3d peak (both $\frac{5}{2}$ and $\frac{3}{2}$ spin-orbit-split peaks of metallic Pd and Pd oxides) is therefore also split into two totalling eight fitted peaks in one spectrum, which is evident in Figs. 1 and 5. In these cases the BE correction was applied to the higher BE peaks of each doublet, therefore the peaks around 332 eV are charging-induced "satellites". The intensity ratio of the two Al 2p peaks is used to split the Pd 3d peaks of each species. The Pd 3d peaks were fitted using fit functions which were customized for each spectrum on the basis of the parameters from the corresponding Al 2p fit, notably peak broadening and splitting. The fit function was designed around the pseudo Voigt function:

$$I(BE) = H\left\{ m \cdot \frac{\tau^2}{2(BE-P)^2+\tau^2} + (1-m) \cdot \exp\left[-\left(\frac{BE-P}{0.601\ \tau} \right)^2 \right] \right\}$$

where BE is the binding energy, P the peak position, H is the peak height, τ the FWHM, and m is the Gaussian–Lorentzian mixing parameter (usually constant at 0.1). The FWHM and mixing parameters are dependent on the corresponding Al 2p spectrum and vary from spectrum to spectrum. The separation between the spin-orbit components Pd $3d_{5/2}$ (low binding energy, 335–337 eV) and Pd $3d_{3/2}$ (high binding energy, 340–342 eV) is always kept fixed at 5 eV (±0.3 eV), as are the relative peak height ratios kept fixed at 1.5 [23, 24]. More information on the fitting procedure, including examples, can be found in the Supporting Information.

Mass spectrometry data were recorded in-situ in order to help quantify methane to syn-gas conversion at different constant temperatures (during the XPS data acquisition) and while cooling down from > 700 K in a 0.33 mbar (240 mTorr) mixture of CH_4 and O_2

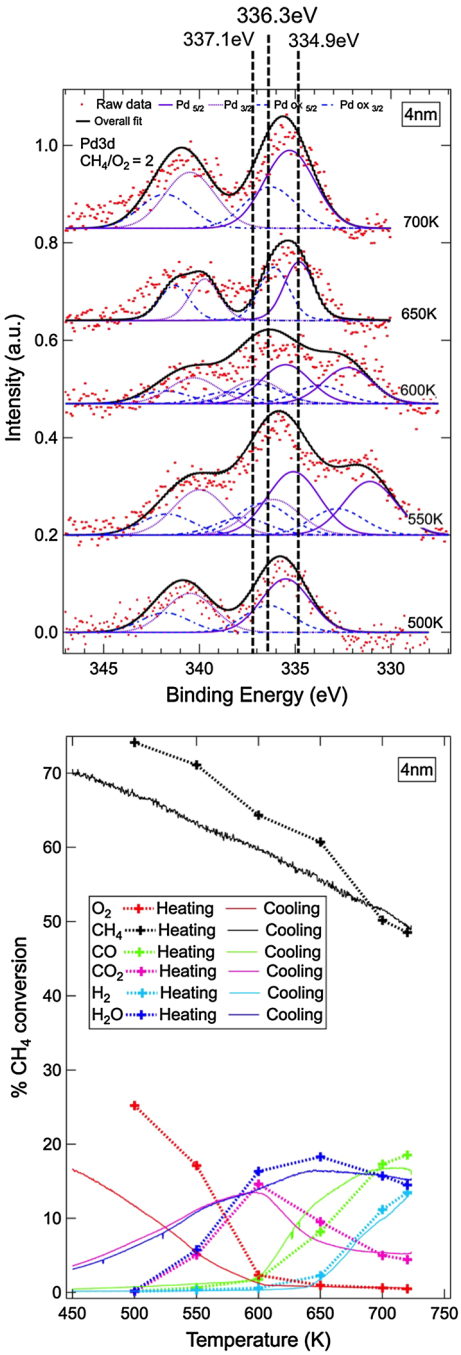

Fig. 1 Catalyst A (Pd/Al_2O_3 nanoparticles of average size 4 nm). NAP-XP spectra in the Pd 3d region (*top*) and CH_4 conversion, calculated from mass spectroscopy data (*bottom*), recorded in the temperature range from 450 to 720 K under 240 mTorr O_2:CH_4 pressure (1:2). "Heating": mass spectrometry at constant temperature during NAP-XPS measurements; "Cooling": recorded during continuous cooling from 720 to 450 K. Binding energies are corrected to corresponding Al 2p spectra at 74.5 eV.

($[CH_4] : [O_2] = 2$). Methane conversion was calculated as the percentage of the partial pressures of each gas observed with respect to the partial pressure of methane at

350 K where no reaction is observed. For example the conversion to CO is:

$$\mathrm{Conv(CO)}_T = \frac{\text{partial pressure of CO at } T}{\text{partial pressure of } CH_4 \text{ at } 350\,\mathrm{K}} \times 100\,\%$$

No correction factors were used to calculate the conversion of each gas.

3 Results

Particle size effects are observed in the near ambient-pressure XP spectra and mass spectrometry data. NAP-XPS in the Pd 3d region is most useful to monitor the chemical state of the metal and therefore the nature of the catalytically active oxide. Figures 1, 2, 3, 4, and 5 show the in-situ data for Catalysts A–E respectively: near ambient-pressure XPS in the Pd 3d region, and the corresponding reactant to product conversion as calculated from mass spectrometry data. High resolution in-situ XPS was taken at 50 K intervals between 500 and 700 K, under 0.33 mbar (240 mTorr) of $CH_4 + O_2$ ($[CH_4] : [O_2] = 2$).

The peaks at lower binding energies (335.0 ± 0.2 eV) are characteristic of metallic Pd (Pd^0) with PdO_x species appearing slightly higher at 336–337 eV. Due to the catalyst preparation method and storage (i.e. exposure to air), Pd shows some degree of oxidation for all samples at 500 K, but metallic Pd peaks at 335.0 ± 0.2 eV are dominant at these lower temperatures. As the temperature is increased to 600 K and again to 650 K, an XPS signal characteristic of a PdO_x species at 336.0–336.2 eV becomes dominant for most particle sizes. The CH_4 conversion plots associated with the NAP-XPS measurements in Figs. 1, 2, 3, 4, and 5, calculated from mass spectrometry data, indicate an increase in syn-gas production around these temperatures. Our activity studies have shown that under similar conditions CH_4 begins conversion to POM products between 550 and 600 K (see Supporting Information). In addition, metallic Pd (335.0 ± 0.2 eV) also has a strong contribution in the XP spectra, and the data show that a mixture of both Pd metal and Pd oxide is needed to continue the reaction, after the oxide has initially been formed. At temperatures above 700 K the oxide species is reduced to metallic Pd and the product formation of CO and H_2 slows down.

The AP-XPS data in Figs. 1, 2, 3, 4, and 5 also show that at 700 K the oxide species is almost fully reduced to metallic Pd. This is reflected in the CH_4 conversion plots which indicate a slowing down of CO and H_2 formation. It could be argued that for Catalyst E (10 nm, Fig. 5) the reaction rate does not slow at 700 K and this could be because a larger ratio of metallic Pd to oxide Pd is present than for other catalysts (see Table 2), further supporting the hypothesis that metallic Pd is key for continuing the reaction.

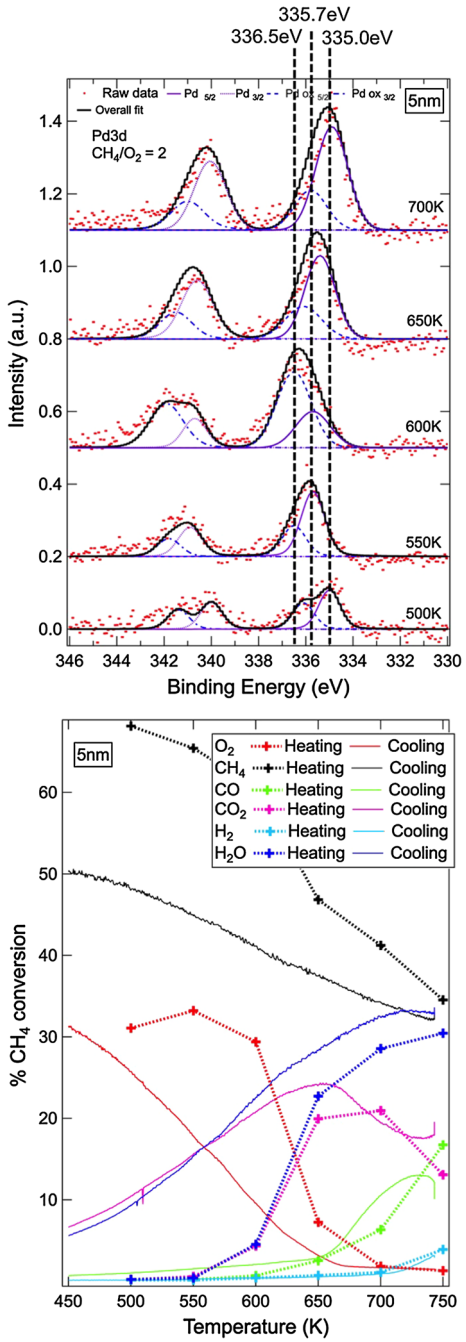

Fig. 2 Catalyst B (Pd/Al_2O_3 nanoparticles of average size 5 nm). NAP-XP spectra in the Pd 3d region (*top*) and CH_4 conversion, calculated from mass spectroscopy data (*bottom*), recorded in the temperature range from 450 to 750 K under 240 mTorr O_2:CH_4 pressure (1:2). "Heating": mass spectrometry at constant temperature during NAP-XPS measurements; "Cooling": recorded during continuous cooling from 750 to 450 K. Binding energies are corrected to corresponding Al 2p spectra at 74.5 eV.

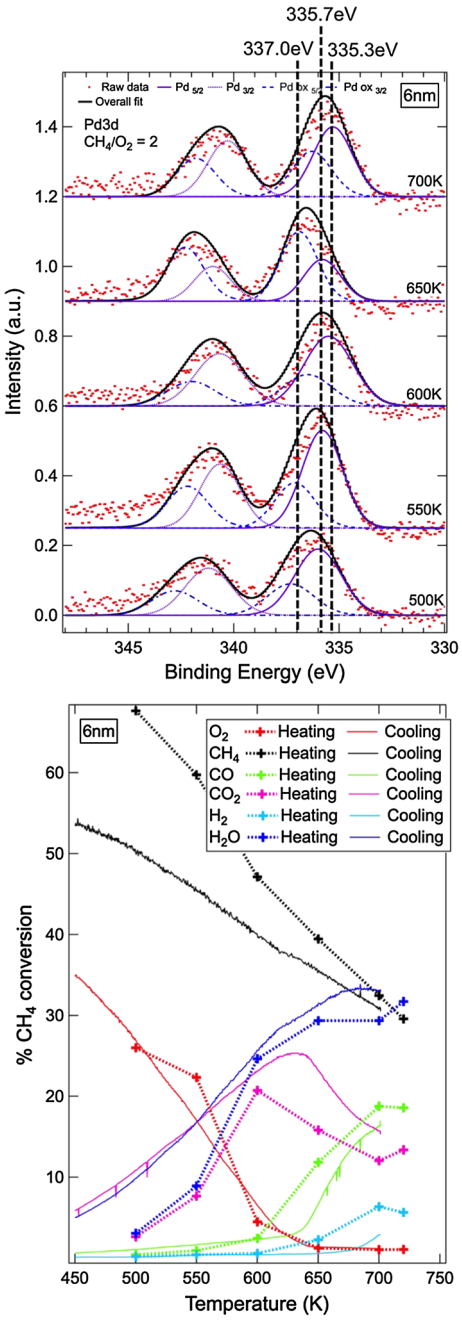

Fig. 3 Catalyst C (Pd/Al_2O_3 nanoparticles of average size 6 nm). NAP-XP spectra in the Pd 3d region (*top*) and CH_4 conversion, calculated from mass spectroscopy data (*bottom*), recorded in the temperature range from 450 to 720 K under 240 mTorr O_2:CH_4 pressure (1:2). "Heating": mass spectrometry at constant temperature during NAP-XPS measurements; "Cooling": recorded during continuous cooling from 720 to 450 K. Binding energies are corrected to corresponding Al 2p spectra at 74.5 eV.

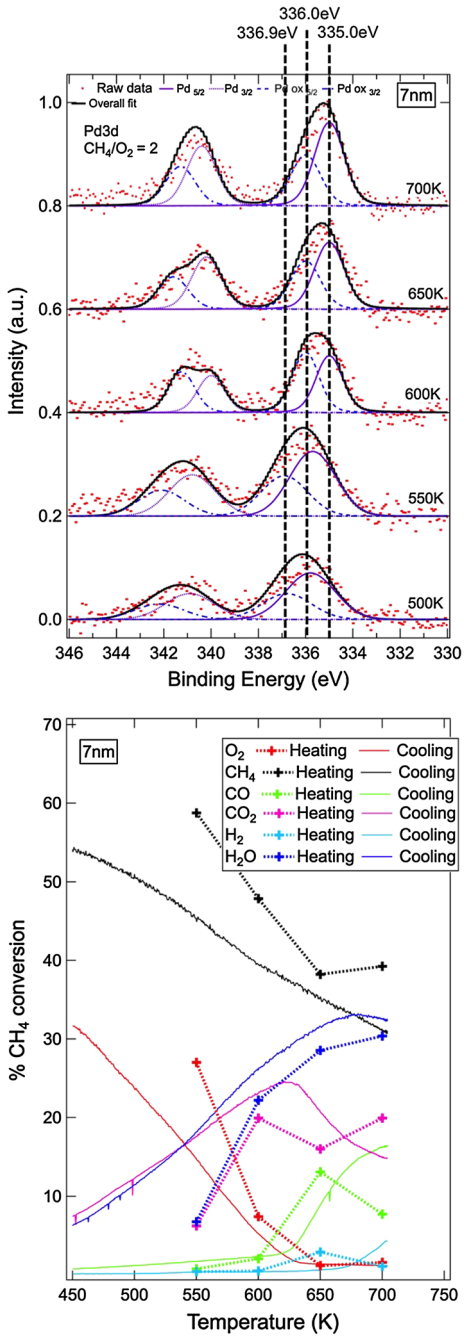

Fig. 4 Catalyst D (Pd/Al_2O_3 nanoparticles of average size 7 nm). NAP-XP spectra in the Pd 3d region (*top*) and CH_4 conversion, calculated from mass spectroscopy data (*bottom*), recorded in the temperature range from 450 to 700 K under 240 mTorr O_2:CH_4 pressure (1:2). "Heating": mass spectrometry at constant temperature during NAP-XPS measurements; "Cooling": recorded during continuous cooling from 700 to 450 K. Binding energies are corrected to corresponding Al 2p spectra at 74.5 eV.

The CH_4 conversion plots in the lower panels of Figs. 1, 2, 3, 4, and 5 show that complete oxidation of methane to CO_2 and H_2O occurs at low temperatures. The selectivity of these catalysts changes towards partial oxidation to syngas at temperatures above 570 K. There is also a distinct difference between catalysts of different sizes with respect to the temperature at which CO and H_2 are produced. Catalyst E (Fig. 5, 10 nm) produces CO and H_2 at the lowest temperature (570 K) and, with the exception of

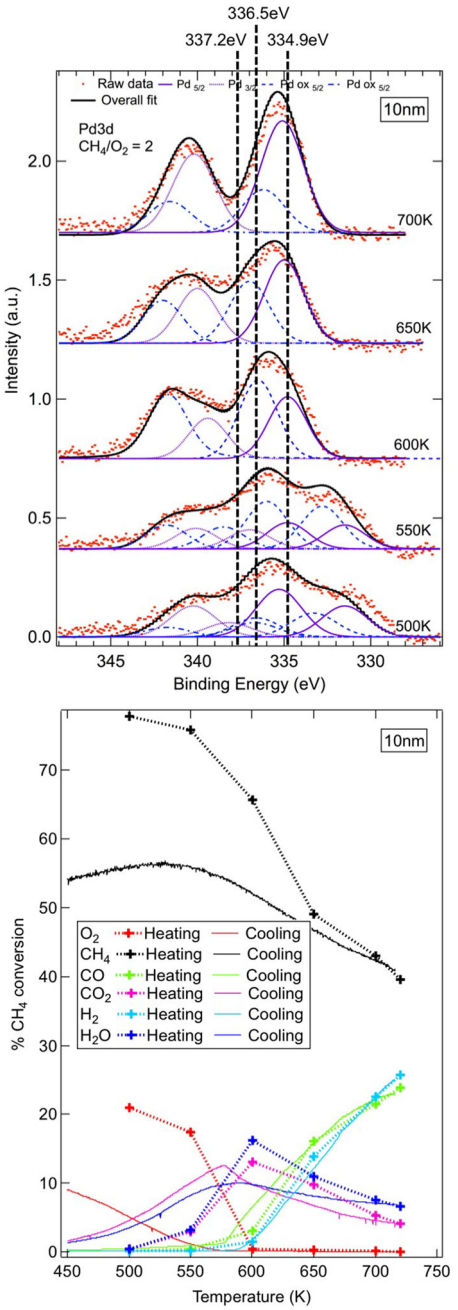

Fig. 5 Catalyst E (Pd/Al_2O_3 nanoparticles of average size 10 nm). NAP-XP spectra in the Pd 3d region (*top*) and CH_4 conversion, calculated from mass spectroscopy data (*bottom*), recorded in the temperature range from 450 to 720 K under 240 mTorr O_2:CH_4 pressure (1:2). "Heating": mass spectrometry at constant temperature during NAP-XPS measurements; "Cooling": recorded during continuous cooling from 720 to 450 K. Binding energies are corrected to corresponding Al 2p spectra at 74.5 eV.

Catalyst A (Fig. 1, 4 nm), the catalytic activity with respect to syn-gas production decreases with decreasing particle size (Fig. 6). The XPS data for Catalyst A (Fig. 1) show a prominent peak at 337.1 eV at 550 and 600 K,

Table 2 Areas of Pd $3d_{5/2}$ metallic Pd and Pd oxide peaks for catalysts A–E at 700 K.

Catalyst	Pd $3d_{5/2}$ Pd area	Pd $3d_{5/2}$ PdO area	Pd:PdO ratio
A (4 nm)	0.5264	0.2804	1.8771
B (5 nm)	0.4853	0.1873	2.5909
C (6 nm)	0.4683	0.3044	1.5384
D (7 nm)	0.2654	0.1632	1.6269
E (10 nm)	1.4498	0.5556	2.6090

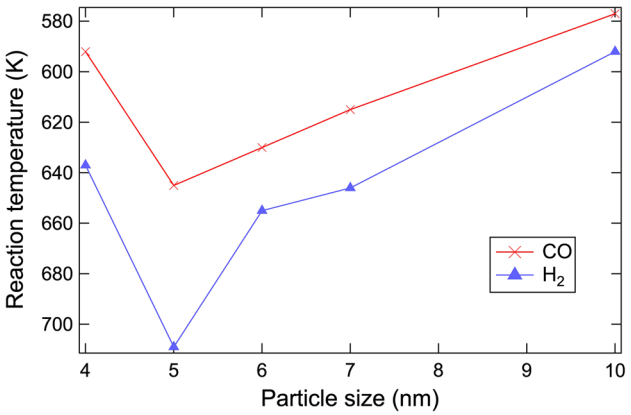

Fig. 6 Temperature of CO and H_2 initial production versus particle size

characteristic of a divalent Pd species (Pd^{2+}) [25]. This peak corresponds to the temperature at which POM products are starting to form according to the mass spectrometry data, suggesting PdO is the active phase of the catalyst. A slight hysteresis is observed, but the process is generally reversible on cooling down. Note, the modes of recording the mass spectrometry data were different: the temperature was increased in steps of 50 K and held constant for about 30 min while the NAP-XP spectra were recorded, after the experiments at the highest temperature (700–750 K) had been completed, the sample was allowed to cool down while recording the reactant and product partial pressures. The NAP-XPS data in Fig. 2 for Catalyst B (5 nm) are slightly different from Catalyst A as the peak at 337.1 eV is not observed. At 600 K, a peak at 336.5 eV appears in the NAP-XP spectrum, which shifts downwards in binding energy with an increase in temperature. Syn-gas (CO and H_2) production, as shown in the conversion plot in Fig. 2, does not occur until 700 K, suggesting the absence of the high binding energy peak (337.0 ± 2 eV) is reflective in the activity of Catalyst B.

In the CH_4 conversion data in Fig. 1 for Catalyst A (4 nm) it can be observed that the increase in CO pressure begins just under 600 K. H_2 is produced around 650 K,

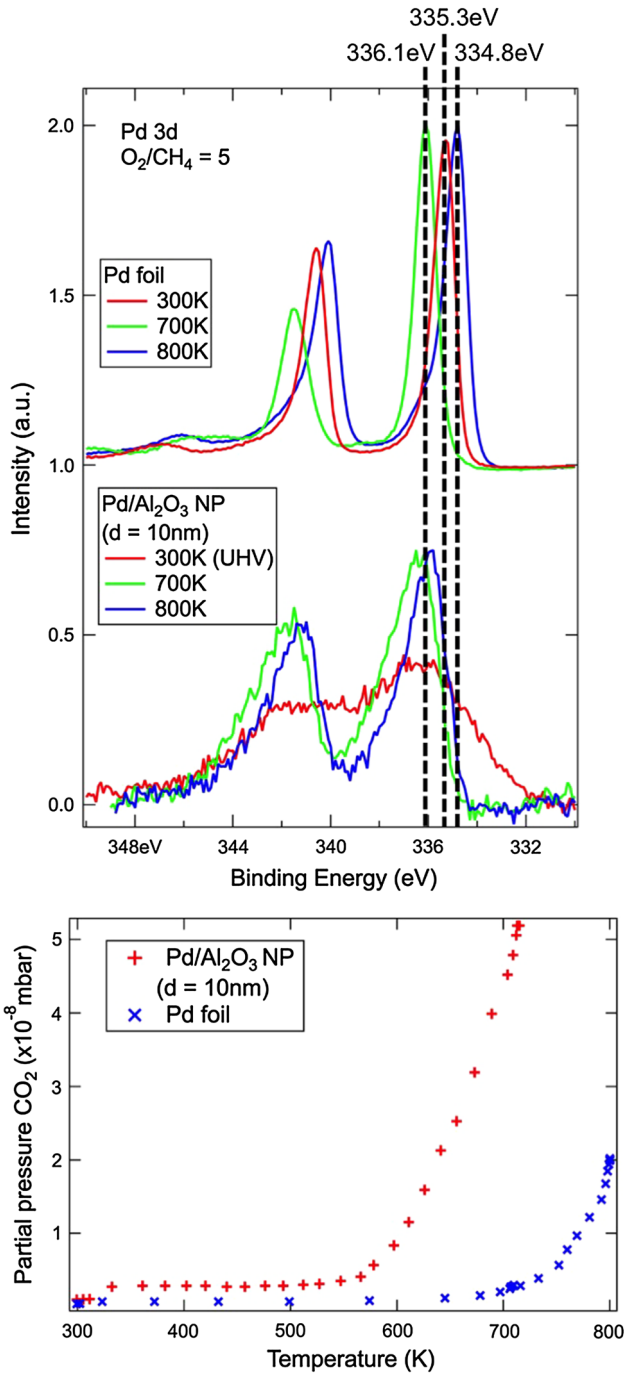

Fig. 7 Comparison of polycrystalline Pd foil and Pd/Al_2O_3 nanoparticles calcined to 600 °C (d = 10 nm): AP-XP spectra and partial pressure of CO_2 produced under O_2/CH_4 = 5 (total gas pressure = 0.33 mbar/240 mTorr) at 300, 700 and 800 K

which can explain why the peak at 334.9 eV reappears as the oxide has been reduced back to Pd^0. In comparing Catalysts C and D (Figs. 3, 6 nm, and 4, 7 nm, respectively), there is a significant temperature dependence at which point the metallic Pd oxidises to the PdO_x species and the reverse reduction. The XPS data shown in Fig. 3 for Catalyst C (6 nm) show the presence of a higher binding energy peak at 337.0 eV (PdO) slowly increasing from 550 to 650 K, whereas the spectra for Catalyst D (7 nm, Fig. 4) show a quick conversion from 336.9 to 336.0 eV between 550 and 600 K. The peak at 336.9 eV in Figure 4 can be attributed to PdO. Its downward shift to 336.0 eV at 600 K could suggest a subsurface oxygen species, a surface 2D oxide such as Pd_5O_4 [26] or even a PdC species [27]. A large peak is observed in the C 1s spectra at 285 eV (see Fig. 6 in Supporting Information). This could be indicative of a PdC surface species, however adventitious carbon from impurities and the reactant gas CH_4 would also appear at this binding energy. Therefore it is impossible to identify whether a surface PdC species is present. C 1s peaks around 292 eV (appearing at 600 K) and at 290 eV (appearing at 650 K) are assigned to gaseous CO_2 and CO, respectively, by comparison with spectra of the gas phase under reaction conditions (see Fig. 7 in Supporting Information). The Pd appears predominately reduced again by 650 K, when the selectivity shifts towards partial oxidation. This can be correlated to the mass spectrometry data, which show that H_2 formation occurs at a lower temperature with Catalyst C (650 K) than with Catalyst D (677 K). XPS data for all catalysts show the reduced species is favoured at 700 K, which is supported by mass spectrometry showing an increase in H_2 formation at much higher temperatures, between 700 and 750 K. Pd/Al_2O_3 nanoparticles with an average diameter of 10 nm (Catalyst E, Fig. 5) also exhibit a PdO species (337.2 eV) that, on heating, reduces to a PdO_x or a subsurface-O species (336.5 eV). This reduction and downward shift in the NAP-XP spectrum occurs between 550 and 600 K, which coincides with the initial formation of CO as the CH_4 conversion plot, shown in Fig. 5, suggests.

4 Discussion and Conclusions

These studies show that the catalytic activity, in terms of the temperature at which CH_4 conversion to CO and H_2 begins, increases with increasing particle size for Pd/Al_2O_3 nanoparticles over a range of particle sizes (5–10 nm). Nanoparticles with an average diameter above 10 nm were not available in this study. Therefore, it is not clear whether there is an optimum particle size or a continuous trend. Pd single crystals and polycrystalline foils have been used as model catalysts in similar AP-XPS studies before [28, 29] however, and show an onset of CO production at higher temperatures. Figure 7 shows the relative CO_2 production of polycrystalline Pd foil compared with Pd/Al_2O_3 nanoparticles when exposed to an oxygen-rich CH_4 environment ($[O_2] : [CH_4] = 5$). In comparison to supported

metallic nanoparticles, the catalytic activity of polycrystalline Pd foil is insignificant. This would suggest that there is a volcano-type distribution of particle size as a function of activity, with an optimum size at some point between 10 nm and the grain size of the polycrystalline foil ($>1\,\mu m$). Other studies using Pd/Al_2O_3 catalysts have also found activity increases with increasing particle size [30, 31], explained by differences in electronic structure of nanoparticles <3 nm that form stronger interactions with the reactant molecules [32]. Similar trends have been reported in the literature [33, 34] for palladium catalysts, in which there is an optimum or critical nanoparticle size for enhanced reactivity when testing a range of particle sizes. Semagina et al. [34] tested a size range of Pd nanoparticles from 6 to 14 nm and Pd black, and found that a significant increase in turnover frequency was observed with nanoparticles of 11–14 nm, but decreased with a Pd black catalyst in the micrometer range. It has also been previously reported that smaller particles have stronger metal-support interactions, which can render them less reactive with the reactant molecules because the palladium content on the surface decreases [35], and conversely, a weaker metal-support interaction makes the catalyst more active [3, 19].

The need for fundamental knowledge of how catalytic nanoparticles behave in-situ is becoming increasingly important. Model catalysts such as polycrystalline foils and single crystals cannot be used to study size effects and metal-support interactions of industrial catalysts. The NAP-XP spectra and mass spectrometry data shown in Fig. 7, are indicative that a polycrystalline Pd foil behaves differently from supported nanoparticles under catalytic reaction conditions. At 700 K, a sharp PdO peak at 336.1 eV in the Pd foil spectrum is consistent with the rise in CO_2 formation shown in Fig. 7. The peaks in the spectra for the nanoparticles are much broader, suggesting a mixture of both oxide and metal, contributing to a rise in catalytic activity at lower temperatures. By 800 K, the Pd foil is further reduced (334.8 eV) [28], whereas the nanoparticles are still predominately in their oxide state (335.9 eV) at this temperature. It could be argued that reactant pressures of around 1 mbar are not representative of industrial catalysis conditions, as syn-gas is currently produced in a large scale reactor at 5–40 bar [36]. However, NAP conditions are considerably more realistic than ultra-high vacuum and reproduce the reaction yields achieved under industrial conditions.

The exact oxidation state of Pd during the reaction cannot be confirmed by XPS measurements alone. PdO_x species have binding energies between 335.5 and 337.0 eV [12, 25, 27]; therefore the exact nature of the oxide is not clear. It could be subsurface oxygen, bulk or surface PdO oxide, or a surface 2D oxide such as Pd_5O_4. These peaks could also indicate a carbon build-up on the Pd surface from the cracking of the reactants and products in the gas phase [37]. The particle size may have a direct impact on the nature of PdO_x, as smaller nanoparticles have increased metal-support interactions, which can in turn affect their thermal stability [38]. This would therefore lead to an increase in binding energy of the Pd $3d_{5/2}$ peak of the PdO_x species in smaller particles (<5 nm). It is probable that more than one oxidation state is present in the oxidised metal, as the fitted XPS peaks are still quite broad over this range and the increasing concentration of newly formed H_2 is simultaneously reducing Pd. Despite this uncertainty in the exact nature of the oxidation state, in-situ XPS shows distinct changes in chemical state of the Pd surface as a function of temperature and a clear correlation with the catalytic activity.

5 Summary

A particle size effect has been observed in Pd/Al_2O_3 nanoparticles catalysing the partial oxidation of methane to syn-gas (CO and H_2). In general, CH_4 conversion to POM products occurs at lower temperatures for larger particles from 5 to 10 nm. NAP-XPS data show the appearance of a metal oxide species around 550–650 K for all particle sizes, whilst mass spectrometry indicates the start of syn-gas production during these temperatures. As H_2 is produced, the oxide species on the Pd surface reduces to metallic Pd by 700 K, slowing down the production of CO. This suggests the formation of the oxide species is the driving force in initial product formation. A mixture of PdO and metallic Pd is needed to maintain the reaction as we observe an increase in intensity of the Pd metal NAP-XPS peaks (335 eV) at the same temperatures at which product formation increases, as shown by mass spectroscopy. A full reduction of the oxide to metal is detrimental to the catalytic process.

Acknowledgments The authors would like to thank the Royal Society of Chemistry and the European Commission for supporting travel to ALS through a Researcher Mobility Fellowship (R.P.) and the COST action CM0904 (R.P. and C.E.), respectively. The Advanced Light Source (ALS) at the Lawrence Berkeley National Laboratory is supported by the Office of Science, Office of Basic Energy Sciences, Scientific User Facilities Division of the US Department of Energy under Contract No. DE-AC02-05CH11231. The authors thank the staff of ALS for their support, in particular Beomgyun Jeong for help with sample mounting and optimising sample position at BL 9.3.2. The authors would also like to thank Johnson Matthey Technology Centre for funding R.P.'s studentship and their staff for help with sample characterisation, in particular Greg Goodlet, Winson Kuo and Dogan Ozkaya (TEM images) and Agnes Raj (reactivity data). Finally, we thank Rosa Arrigo (Diamond Light Source) for helpful discussions and help with data analysis.

References

1. Gelin P, Primet M (2002) Appl Catal B 39:1–37
2. Burch R, Urbano F (1995) Appl Catal A 124:121–138
3. Gannouni A, Albela B, Zina MS, Bonneviot L (2013) Appl Catal B 464–465:116–127
4. Enger B, Lodeng R, Holmen A (2008) Appl Catal A 346:1–27
5. Cai Y, Niu Y, Chen Z (1997) Fuel Process Technol 50:163–170
6. Li K, Jiang D (1999) J Mol Catal A 147:125–130
7. Holmen A (2009) Catal Today 142:1–98
8. Chen Y, Wang Y, Xu H, Xiong G (2008) Appl Catal B 80:283–294
9. Claridge J, Green M, Tsang S, York A, Ashcroft A, Battle P (1993) Catal Lett 22:299–305
10. Vernon P, Green M, Cheetham A, Ashcroft A (1990) Catal Lett 6:181–186
11. Zhu Y, Zhang S, Shan J, Nguyen L, Zhan S, Gu X, Tao F (2013) ACS Catal 3:2627–2639
12. Teschner D, Pestryakov A, Kleimenov E, Havecker M, Bluhm H, Sauer H, Knop-Gericke A, Schlögl R (2005) J Catal 230:186–194
13. Burch R, Crittle D, Hayes M (1999) Catal Today 47:229–234
14. Yang S, Maroto-Valiente A, Benito-Gonzalez M, Rodriguez-Ramos I, Guerrero-Ruiz A (2000) Appl Catal B 28:223–233
15. Lundgren E, Kresse G, Klein C, Borg M, Andersen J, Santis MD, Gauthier Y, Konvicka C, Schmid M, Varga P (2002) Phys Rev Lett 88:246103
16. Kaya S, Ogasawara H, Naslund L, Forsrell J-O, Casalongue H, Miller D, Nilsson A (2013) Catal Today 205:101–105
17. Schnadt J, Knudsen J, Andersen J, Siegbahn H, Pietzsch A, Hennies F, Johansson N, Martensson N, Ohrwall G, Bahr S, Mahl S, Schaff O (2012) J Synchrotron Radiat 19:701–704
18. Pinna F (1998) Catal Today 41:129–137
19. Ivanova A, Slavinskaya E, Gulyaev R, Zaikovskii V, Stonkus O, Danilova I, Plyasova L, Polukhina I, Boronin A (2010) Appl Catal B 97:57–71
20. Grass M, Karlsson P, Aksoy F, Lundqvist M, Wannberg B, Mun B, Hussain Z, Liu Z (2010) Rev Sci Instrum 81:053106
21. Shirley D (1972) Phys Rev B 5:4709
22. Strohmeier B (1994) Surf Sci Spectra 3:141
23. Zemlyanov D, Aszalos-Kiss B, Kleimenov E, Teschner D, Zafeiratos S, Havecker M, Knop-Gericke A, Schlögl R, Gabasch H, Unterberger W, Hayek K, Klotzer B (2006) Surf Sci 600:983–994
24. Griffith W, Robinson S (2013) Pd palladium: palladium compounds. Springer, Berlin
25. Arrigo R, Schuster M, Xie Z, Yi Y, Wowsnick G, Sun L, Hermann K, Friedrich M, Kast P, Havecker M, Knop-Gericke A, Schlögl R (2015) ACS Catal
26. Gabasch H, Hayek K, Klotzer B, Unterberger W, Kleimenov E, Teschner D, Zafeiratos S, Havecker M, Knop-Gericke A, Schlögl R, Aszalos-Kiss B, Zemlyanov D (2007) J Phys Chem C 111:7957–7962
27. Teschner D, Borsodi J, Wootsch A, Revay Z, Havecker M, Knop-Gericke A, Jackson SD, Schlögl R (2008) Science 320:86
28. Monteiro R, Zemlyanov D, Storey J, Ribeiro F (2001) J Catal 199:291–301
29. Gabasch H, Unterberger W, Hayek K, Klotzer B, Kleimenov E, Teschner D, Zafeiratos S, Havecker M, Knop-Gericke A, Schlögl R, Han J, Riberio F, Aszalos-Kiss B, Curtin T, Zemlyanov D (2006) Surf Sci 600:2980–2989
30. Boitiaux J, Cosyns J, Vasudevan S (1983) Appl Catal 6:41–51
31. Tardy B, Noupa C, Leclercq C, Bertolini J, Hoareau A, Treilleux M, Faure J, Nihoul G (1991) J Catal 129:1–11
32. Silvestre-Albero J, Rupprechter G, Freund H-J (2006) J Catal 240:58–65
33. Ota A, Kunkes E, Krohnert J, Schmal M, Behrens M (2013) Appl Catal A 452:203–213
34. Semagina N, Renken A, Kiwi-Minsker L (2007) J Phys Chem C 111:13933–13937
35. Ji L, Lin J, Zeng HC (2000) J Phys Chem B 104:1783–1790
36. Lyubovsky M, Roychoudhury S, LaPierre R (2005) Catal Lett 99:113–117
37. Bychkov V, Tyulenin Y, Slinko M, Shashkin D, Korchak V (2009) J Catal 267:181–187
38. Suhonen S, Valden M, Pessa M, Savimäki A, Härkönen M, Hietikko M, Pursiainen J, Laitinen R (2001) Appl Catal A 207:113–120